ELSEVIER

Chemical Engineering Science 60 (2005) 1743–1759

Chemical Engineering Science

www.elsevier.com/locate/ces

The dynamic response of PEM fuel cells to changes in load

Jay Benziger*, E. Chia, J.F. Moxley, I.G. Kevrekidis

Department of Chemical Engineering, Princeton University, Princeton, NJ 08544, USA

Received 25 February 2004; received in revised form 7 October 2004; accepted 7 October 2004

Abstract

The dynamic response of the stirred tank reactor (STR) polymer electrolyte membrane (PEM) fuel cell has been explored over the temperature range of 35–105 °C. When the fuel cell was operated in the autohumidification mode the fuel cell current "ignited" when the membrane water content was greater than a critical level of ~1.6 H_2O/SO_3, and it extinguished when the initial membrane water content was below this critical level. Above 70 °C, two stable "ignited" states were observed at intermediate load resistances; these steady states corresponded to different levels of membrane hydration. At low load resistances only a single ignited steady state was observed with high membrane hydration, and at high load resistances only a single ignited steady state was observed with intermediate membrane hydration. Hysteresis between the two ignited states was observed; the steady state selected depended on the initial conditions in the fuel cell. The time constant for the fuel cell current to reach steady state after a change in the load resistance was $\sim 10^3$–10^4 s. Below 70 °C only one "ignited" state and the extinguished state were observed in the autohumidification fuel cell. After 3000 h of operation the STR PEM fuel cell current and effluent relative humidities oscillated autonomously between two membrane hydration states with a period of oscillation of ~10,000 s. The oscillations showed abrupt transitions indicative of a capacitive switch. These complex dynamics of PEM fuel cell operation are associated with the membrane water uptake. It is hypothesized that water produced and swells the membrane, altering the interfacial membrane–electrode contact.

Keywords: Fuel cells; Multiphase reactors; Nonlinear dynamics; Reaction engineering; Polymer swelling

1. Introduction

Polymer electrolyte membranes (PEM) mediate the transport of protons between the anode and cathode in PEM fuel cells. Membrane humidification is essential for ion transport in the fuel cell. If the membrane is not adequately humidified the proton conductivity is low and the power output from the fuel cell is limited. At the other extreme, too much water can flood the electrodes with liquid, hindering gas transport to the catalyst/membrane interface, also limiting the power output from the fuel cell. We previously reported the existence of a critical initial membrane water content capable of "igniting" a PEM fuel cell (Moxley et al., 2003). We demonstrated a positive feedback between water production and membrane water activity that resulted in multiple steady states in the autohumidification PEM fuel cell.

The essential result from this previous work was that *the PEM is a reservoir for water, and the membrane resistance depends on the water inventory in the membrane*. Changes in the operating parameters of the PEM fuel cell, such as the external load resistance or the fuel cell temperature, alter the balance between water production and water removal, thereby changing the membrane water activity.

This paper reports dynamical results of the differential stirred tank reactor (STR) PEM fuel cell to changes in load and in temperature. This paper is organized as follows: the ignition phenomenon in a PEM fuel cell is reviewed as the starting point for studying dynamics. The dynamical responses to changes in external load resistance are reported, suggesting a coupling of the mechanical properties of the membrane to its chemical and transport properties. This coupling of mechanical and chemical properties gives rise to

* Corresponding author. Tel.: +1 609 258 5416; fax: +1 609 258 0211.
E-mail address: benziger@princeton.edu (J. Benziger).

0009-2509/$ - see front matter © 2004 Elsevier Ltd. All rights reserved.
doi:10.1016/j.ces.2004.10.033

highly unusual responses, including the existence of 5 steady states in PEM fuel cells, and the occurrence of autonomous oscillations with extremely long periods, ∼10,000 s. Lastly, we suggest how our observations may be employed to improve PEM fuel cell design.

2. Experimental

Experiments were carried out in a differential STR PEM fuel cell described elsewhere (Moxley et al., 2003; Benziger et al., 2004). The STR PEM fuel cell is a one-dimensional differential reactor where the only gradients are transverse, across the PEM. The fuel cell can be modeled as two well mixed reactors coupled through the PEM. The membrane–electrode-assembly (MEA) was pressed between two machined graphite plates and sealed with a silicon rubber gasket. Gas flow channels at the anode and cathode were replaced with plenums above the MEA. The plenums were open areas of about 1 cm × 0.2 cm deep. There were pillars in the plenums to apply pressure more uniformly across the MEA. The active area of the MEA was $\sim 1\,\mathrm{cm}^2$. Hydrogen and oxygen were supplied from commercial cylinders (Airco) through mass flow controllers at flow rates, $Q \sim 1$–$10\,\mathrm{cm}^3/\mathrm{min}$ (mL/min). The residence times of the reactants in the gas plenums ($V/Q = 1.2$–12 s) were greater than the characteristic diffusion time ($V^{2/3}/D = 0.3$–1.0), ensuring uniformity of the gas compositions at both the anode and cathode. The cell temperature was controlled by placing the graphite plates between aluminum plates fitted with cartridge heaters connected to a temperature controller. The entire fuel cell assembly was mounted inside an aluminum box to maintain temperature uniformity.

Gas pressure was maintained in the cell by placing spring loaded pressure relief valves (Swagelok) at the outlets. Tees were placed in the outlet lines with relative humidity sensors in the dead legs of the tees. The water content of the outlet streams was measured with humidity sensors (Honeywell HIH 3610), and the temperature at the humidity sensors was measured with a thermocouple in the gas line. At a flow rate of $10\,\mathrm{cm}^3/\mathrm{min}$ the humidity sensor responded to changes in the humidity at the anode and cathode in < 2 s.

We report here results using an MEA consisting of a Nafion™ 115 membrane pressed between 2 E-tek electrodes (these consist of a carbon cloth coated on one side with a Pt/C catalyst). The catalyst weight loading at each electrode was $0.4\,\mathrm{mg\text{-}Pt/cm}^2$. Each electrode was brushed with solubilized Nafion solution to a loading of $\sim 4\,\mathrm{mg\text{-}Nafion/cm}^2$ before placing the membrane between them (Raistrick, 1989). The assembly was hot pressed at 130 °C and 10 MPa. Copper foils were pressed against the graphite plates and copper wires were attached to connect them to the external load resistor.

The current and voltage across the load resistor were measured as the load resistance was varied. A 10-turn 0–20 Ω potentiometer was varied to obtain a polarization curve (IV curve). Current and voltage were both read out by a data acquisition board and stored by computer. For transient studies the current, voltage and relative humidity of the anode and cathode effluents were read out by computer and stored.

The STR PEM fuel cell was normally operated in the autohumidification mode; it performed continuously for hundreds of hours without attention. The data presented in this paper were obtained with three different MEAs. The first MEA was operated for a period of ∼2000 h; the membrane failed after 2000 h and the open circuit voltage fell to zero. When the fuel cell was opened, a rip was found in the membrane along the sealing surface of the graphite plates. A second MEA was employed with the flow channel plate modified, so it had open plenums at the anode and cathode and no pillars to seal the MEA at the center. The initial performance of this MEA was similar to the first, but the fuel current density at the same operating conditions fell to 25% of the first MEA after 200 h. We replaced that MEA/flow channel plate assembly with a replica of the original design. The third MEA assembly was operated continuously for ∼12,000 h. During the first 2000 h of operation the open circuit voltage was 0.92 V, comparable to the first MEA. The polarization curves taken with the first and third MEA were reproducible within 0.05 V.

The fuel cell was operated autonomously, without external control. The independent system parameters for the fuel cell are the feed flow rates, feed gas composition, fuel cell temperature and *external load resistance*. *We present data with the external load resistance as the independent parameter. This is different from the traditional electrochemistry approach where PEM fuel cells are operated under galvanostatic or potentiostatic control* (*constant current or constant voltage*). We wish to understand the *autonomous* operation of the PEM fuel cell; operation of the fuel cell under galvanostatic or potentiostatic *control* can distort the autonomous dynamics. The feed flow was also fixed and was not slaved to the current as is frequently done in fuel cell operation. Most experiments were carried out with a hydrogen flow rate of $10\,\mathrm{cm}^3/\mathrm{min}$, which limited the current to ∼680 mA. In most instances the currents in our experiments were < 200 mA.

In the results presented here we have limited ourselves to conditions where liquid water is not present in the fuel cell (relative humidity is kept below 100%). When liquid water condensed in the fuel cell, it operated irregularly. The gas flow would change erratically due to water droplets blocking the effluent. The irregular operation of the PEM fuel cell with liquid water formation is highly relevant to the fuel cell pathology, but it lies beyond the scope of this paper.

The dynamics of the STR PEM fuel cell are much simpler to analyze than experiments performed with a typical fuel cell test station. The STR PEM fuel cell is one-dimensional, so the current, voltage and membrane resistance are all spatially uniform. The water content only varies transverse to the membrane. All the system variables may be directly related to the anode and cathode effluent compositions. No

spatial integration of the current density, or membrane water content is necessary.

3. Steady state multiplicity in a PEM fuel cell

Ignition/extinction is indicative of multiple steady states in PEM fuel cell operation (the same reactor conditions, feed flow rates, temperature and load resistance can result in two different stable operating states). Steady state multiplicity in the autohumidification PEM fuel cell results from a positive feedback between water production and the membrane resistance (Moxley et al., 2003; Chia et al., 2004). The fuel cell reaction to produce water is limited by the proton conductivity of the polymer electrolyte. Some of the water produced by reaction is absorbed by the membrane decreasing its resistance. The lower resistance permits a greater proton current, which leads to more water production. The feedback loop for ignition by water in the STR PEM fuel cell is analogous to the classic thermal ignition phenomenon (van Heerden, 1953; Uppal et al., 1974).

The membrane resistance for proton conduction decreases exponentially with water activity in the membrane, a_w; the experimental data for Nafion 115 is fit very well with the expression, $R_m = 10^7 * \exp(-14(a_w)^{0.2})\,\Omega$-cm (Yang et al., 2004). At steady state there is a balance between water produced in the fuel cell and water removed by convective flow out of the fuel cell.

$$\frac{F_A^{\text{out}} P_w^A(a_w) + F_C^{\text{out}} P_w^C(a_w)}{\mathscr{F} RT} = 0.5 i_{\text{H}^+} = \frac{0.5V'}{R_m(a_w) + R_L}. \quad (1)$$

The F's are volume flow rates, P's are the water partial pressures, $\mathscr{F}$ is Faraday's constant and i_{H^+} is the current. The fuel cell current equals an *effective cell voltage*, V', divided by the sum of the load resistance and membrane resistance. We define the effective cell voltage as the open circuit voltage less the activation overpotential. In the linear or ohmic region of the polarization curve, V' is approximately constant with a value of 0.85–0.9 V (Springer et al., 1991; Srinivasan et al., 1993; EG&G Services, 2000). The membrane resistance decreases exponentially with increasing water activity, which results in the proton current being a sigmoidal function of membrane water activity, as illustrated in Fig. 1. The water activity in the gas phases at the anode and cathode are equal to the water partial pressure, P_w, divided by the water vapor pressure, P^0. The water activity in the membrane is equal to the partial pressure of water in equilibrium with the water in the membrane divided by the water vapor pressure at the operating temperature.

Water removal and water production are balanced at steady state. Water production and removal can be expressed as functions of the water activity in Eq. (1), and steady state can be represented by the intersections of water production and removal curves. Water removal is represented by the left-hand side of Eq. (1); it consists of water evaporating from the membrane into the effluent streams. The water removal rate is approximately a straight line in Fig. 1, whose slope increases with temperature. Water production is given by the right-hand side of Eq. (1), and is plotted with load resistance as a second parameter. Membrane resistance at constant water activity is essentially insensitive to temperature, so the water production curves are more or less independent of temperature when plotted as a function of water *activity* (this would not be the case if water partial pressure was employed as the independent variable in Fig. 1). In essence, *water production is controlled by the external load resistance and water removal is controlled by temperature and flow rate*! Fixing the load resistance, feed flow rates and cell temperature results in either one or three intersections of the water production and water removal curves, corresponding to steady states. At a high load resistance and high temperature there is a single low current or "extinguished'' steady state. At moderate load resistances and low temperatures, three steady states exist. In addition to the extinguished state, there exists a high current or "ignited'' steady state, and an intermediate steady state.

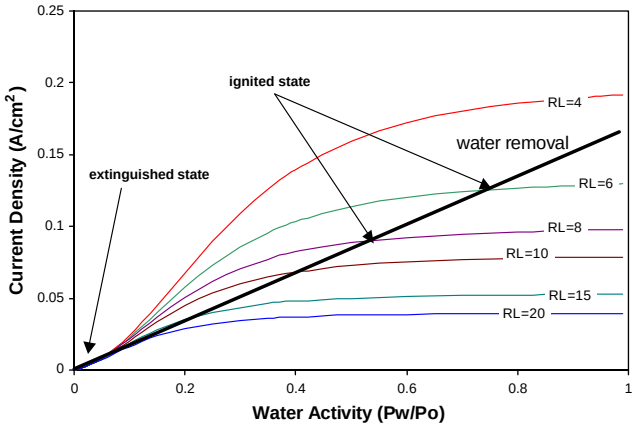

Fig. 1. Water production and removal in an autohumidification STR PEM fuel cell. The curves are based on the model equations given in Eq. (1). The sigmoidal curves show water production for different external load resistances, given by the right-hand side of Eq. (1). The straight line is the water removal by convection, given by the left-hand side of Eq. (1). The intersections of the water production and water removal curves represent steady states.

The dynamics of startup of an autohumidification PEM fuel cell at 50 °C with an external load resistance of 5 Ω and fixed initial water content of the membrane were previously reported (Moxley et al., 2003; Benziger et al., 2004). When the initial membrane water content was below a critical level (< 1.7 H_2O/SO_3) the fuel cell eventually approached the extinguished state, where the steady state current is very low ($\sim 0.1\,\text{mA/cm}^2$). When the initial membrane water loading was above the critical level the fuel cell "ignited'' and approached a "high current'' steady state of $\sim 125\,\text{mA/cm}^2$.

The steady state conditions in an autohumidification STR PEM fuel cell were determined as functions of temperature

Table 1
Autohumidification PEM fuel cell performance

Cell temperature (°C)	Load resistance (Ω)	Steady state current (mA/cm^2)*	Water removed at anode (nmol/cm^2-s)	Water removed at cathode (nmol/cm^2-s)
35	0.5	Unstable**		
	7.5	64 (332)	150	184
	15	31 (161)	71	92
50	0.5	Unstable**		
	5	80 (415)	187	240
	15	32 (166)	68	96
65	0.5	176 (912)	407	522
	5	78 (404)	166	246
	15	31 (161)	66	100
80	0.5	145 (751)	302	440
	5	76 (394)	152	245
	15	15 (78)	26	58
95	0.5	130 (674)	226	440
	5	72 (373)	116	252
	15	12 (62)	18	52
105	0.5	54 (280)	85	180
	5	31 (161)	45	125
	15	<1	<5	<5

*Values in parentheses is the water production rate in nmol/cm^2-s.
**Unstable operation—the humidity sensors were pegged and the current was irregular.

from 35 to 105 °C and load resistances from 0.5 to 15 Ω. In each test the fuel cell was conditioned by setting the temperature, reducing the load resistance to 0.5 Ω, and permitting the fuel cell to stabilize for >2 h. The load resistance was then set to the desired value and the fuel cell was allowed to stabilize for >4 h. The current through the external load, voltage across the external load, temperature of the fuel cell and relative humidity of the anode and cathode effluents were recorded.

The relative humidity (RH) readings of the effluents from the anode and cathode were converted to mole fractions in each stream, x_w through global mass balances (Eq. (2)). The molar flow rates of the feed are F^{in}(mol/s), i_{H^+} is the cell current (amp), $\mathscr{F}$ is Faraday's constant (coulomb/mol), and ξ is the fraction of water that exits in the anode effluent (the water is formed at the cathode and must diffuse through the membrane to be transferred to the anode effluent).

$$x^A_{H_2O} = \frac{P^0_{H_2O}\left(\frac{RH_{\text{anode}}}{100}\right)}{P_{\text{Total}}} = \frac{\xi \cdot i_{H^+}/2\mathscr{F}}{F^{\text{in}}_A + \xi \cdot i_{H^+}/2\mathscr{F} - i_{H^+}/2\mathscr{F}},$$
$$x^C_{H_2O} = \frac{P^0_{H_2O}\left(\frac{RH_{\text{cathode}}}{100}\right)}{P_{\text{Total}}} = \frac{(1-\xi) \cdot i_{H^+}/2\mathscr{F}}{F^{\text{in}}_C + (1-\xi) \cdot i_{H^+}/2\mathscr{F} - i_{H^+}/2\mathscr{F}}. \quad (2)$$

Eq. (2) are solved for ξ knowing the molar flow of the feed, the total pressure, the saturation vapor pressure of water (determined from the effluent temperature) and relative humidity in each of the effluent streams. The value of ξ was determined from the mass balances at both the anode and cathode and checked for consistency to be the same within 5%. The water removal rates at the anode and cathode are given by the molar flows of the effluents multiplied by the mole fraction of water in the effluent streams, and are given by Eq. (3).

$$F^{\text{out}}_{A,H_2O} = \xi \cdot i_{H^+}/2\mathscr{F},$$
$$F^{\text{out}}_{C,H_2O} = (1-\xi) \cdot i_{H^+}/2\mathscr{F}. \quad (3)$$

Table 1 summarizes the steady state current and water removal from both the anode and cathode as functions of the load resistance and temperature. All these data are steady states—the fuel cell was operated in excess of 4 h for the conditions tabulated to verify steady state operation. In particular the conditions at 95 and 105 °C were tested continuously for over 100 h to verify the steady state operation. The results in Table 1 show that the PEM fuel cell was operated in an autohumidification mode over a wide temperature range (35–105 °C), with varying load resistances. All these steady states can be characterized as "ignited" except for operation at 105 °C with a 15 Ω load resistance, where the fuel cell current was extinguished. The fuel cell did not operate stably at either 35 or 50 °C with a low external resistance. At those conditions the relative humidity sensors were pegged at ~100% RH and the fuel cell current and voltage were erratic. We believe at those conditions liquid water condensed in the fuel cell and caused flooding. At all the other conditions the water vapor pressure in the both the

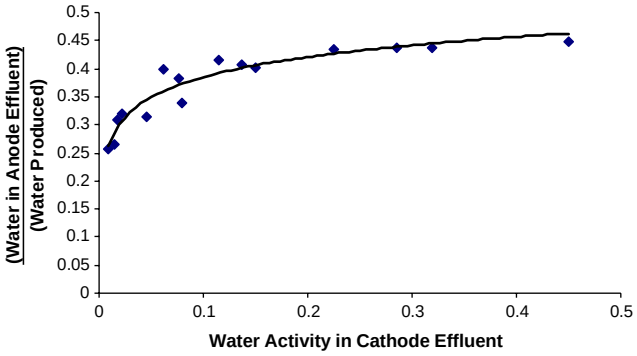

Fig. 2. The fraction of water produced in the fuel cell that exited in the anode effluent as a function of the water activity in the cathode effluent. These data were obtained for the autohumidification STR PEM fuel cell. The water activity in the cathode effluent was varied by changing the external load resistance, which changed the amount of water produced in the fuel cell.

anode and cathode effluents was less than 100% RH, therefore, no liquid water was present at the anode and cathode.

Water was formed at the cathode and either evaporated and exited in the cathode effluent or diffused through the membrane and exited in the anode effluent. The fraction of water exiting at the anode varied from 0.25 to 0.45. These amounts of water removed at the anode are comparable to results obtained by Buchi and Srinivasan (1997) for an autohumidified PEM fuel cell with high hydrogen stoichiometry (low hydrogen utilization). The water partitioning appears to increase with the water activity at the cathode; Fig. 2 shows that the fraction of water exiting in the anode stream increased with the water activity of the cathode effluent. No trends in the water partitioning were observed with the variation of cell temperature.

4. More steady states

The model for fuel cell ignition suggested that the ignited steady state could be extinguished by raising the fuel cell temperature or increasing the load resistance. Testing this hypothesis produced a surprising result. The STR PEM fuel cell was operated in the autohumidification mode at 95 °C with an anode feed of 10 mL/min H_2 and a cathode feed rate of 10 mL/min O_2. The fuel cell was allowed to come to steady state with a load resistance of $\sim 0.2\,\Omega$ for 24 h. The load resistance was then increased stepwise by $\sim 1\,\Omega$ and the fuel cell current and voltage were permitted to stabilize for 3–4 h, after which the current and voltage were recorded. The current/voltage data are plotted as the "steady state" polarization curve in Fig. 3A. The water activity at the cathode and anode change along the steady state polarization curve, reflecting the altered balance between water production and water removal as the load resistance is varied. Steady state polarization curves must allow sufficient time for the membrane water content to equilibrate with the water production and removal; equilibration may take many hours depending on the change in load, the reactant flow rates and the temperature. The curvature of the polarization curve is the result of the water activity at the cathode increasing with the decreasing load resistance.

The steady state polarization curve showed that the current decreased smoothly and the voltage increased smoothly as the load resistance was increased from 0.2 to 11 Ω. When the load resistance was increased from 11 to 12 Ω both the steady state current and voltage decreased abruptly, but the fuel cell did not extinguish. The resistance was then increased stepwise from 12 to 20 Ω and the current decreased and voltage increased smoothly, but along a different trajectory. Starting with a load resistance of 20 Ω, the process was reversed and the load resistance was decreased stepwise by $\sim 1\,\Omega$ every 3–4 h. The current and voltage followed the same trajectory as seen for the high load resistance polarization curve, but there was no abrupt change in the current and voltage at 11 Ω. Instead the IV data varied smoothly until the resistance was decreased below 5 Ω, when it jumped to match the polarization curve taken with decreasing load resistance.

The polarization curves in Fig. 3A show a hysteresis loop, where the steady state current and voltage depend on the direction of approach. It was possible to go around the hysteresis loop shown in Fig. 3A reproducibly many times. When the load resistance was between 5 and 11 Ω the steady state current and voltage were dependent on the direction of approach. These multi-valued steady states were stable; the current and voltage at any point on the steady state polarization curve was steady for periods of > 24 h. We also did a control experiment to verify the existence of an extinguished state. The membrane was dried by operating the fuel cell at 95 °C and open circuit (infinite load resistance) for 48 h. The load resistance was switched to 5 Ω; the fuel cell current never increased and was < 1 mA for more than 48 h.

The steady state polarization curve shown in Fig. 3A shows regions where there are either 1, 2 or 3 *stable* steady states that could exist for the same set of operating parameters (feed flow rate, temperature and load resistance). On an IV plot, rays from the origin correspond to fixed load resistance (the slope of the ray is the load resistance). The intersection of the ray from the origin with the polarization curve represents the steady state current and voltage corresponding to a specified load resistance. One steady state corresponds to an extinguished state where the current and voltage are both near zero; this occurs for very large load resistances. When the load resistance is sufficiently small there are two stable steady states, the extinguished state near the origin and an ignited state. At intermediate load resistances the rays from the origin intersect the polarization curve at two ignited states and the extinguished state. We refer to the three stable steady states by the relative water content in the membrane as inferred from the membrane/electrode resistance, and the water activity in the anode effluent. The three stable steady states are the dry state (extinguished current),

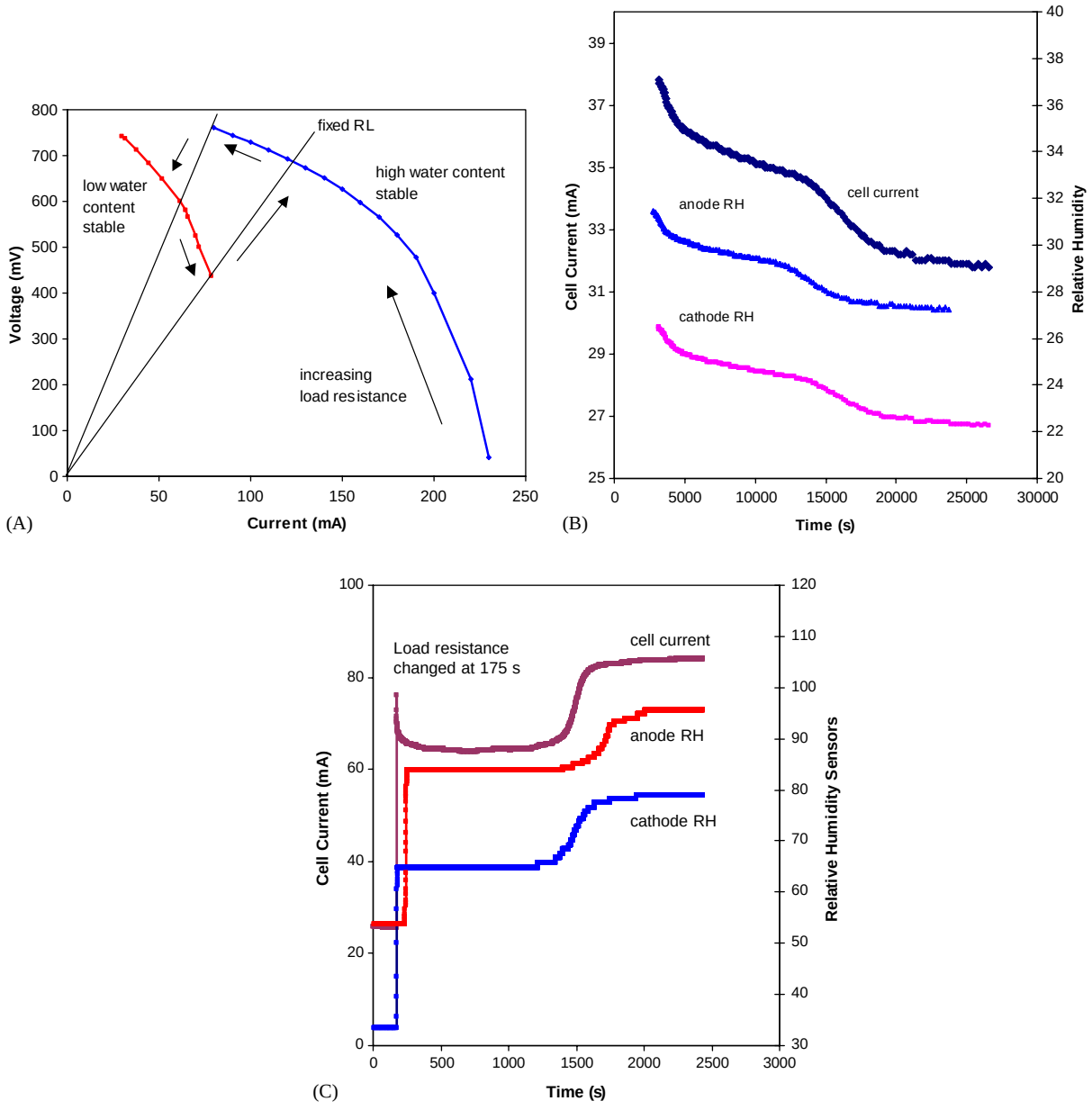

Fig. 3. (A) Steady state polarization curves for autohumidification PEM fuel cell at 95 °C with H_2 flow and O_2 flow of 10 mL/min. The high water content curve was taken after establishing steady state with a load resistance of 2 Ω. The low water content curve was taken after establishing steady state with a load resistance of 20 Ω. (B) Fuel cell current at 95 °C and relative humidity response to a step increase in the load resistance from 2 to 20 Ω. The change was made at 3300 s. The current from 0 to 3300 s was 175 mA. (C) Fuel cell current at 95 °C and relative humidity in the anode and cathode effluents in response to a step decrease in the external load resistance from 25 to 5 Ω. The switch was made at 175 s.

low water content state (intermediate current) and high water content state (high current).

The dynamics of the transitions that accompany changes in load are unusual, and they demonstrate the importance of waiting for sufficiently long time for the fuel cell to equilibrate to attain steady state. Shown in Figs. 3B and C are the responses of the current and relative humidity in the anode and cathode effluent to a step change in the external load resistance. The resistance value was chosen to be outside the hysteresis loop shown in Fig. 3A. As depicted in Fig. 3C, when the load resistance was reduced from 25 to 5 Ω the current jumped immediately from 25 to 75 mA, and then settled at 65 mA within seconds. The current remained steady at 65 mA for almost 1500 s; after 1500 s the current jumped to 87 mA over the course of ∼100 s, where it remained steady for a period of more than 24 h. The approach to steady state when the load resistance was changed from a low load resistance (2 Ω) to a high load resistance (20 Ω) took a longer time, ∼10,000 s, as shown in Fig. 3B. The water content in the effluent streams, as measured by the

relative humidity, also tracked the current changes. These results show there exist dynamic processes in the PEM fuel cell operation associated with at least three distinct time scales: processes that respond in < 1 s, processes that respond in ~ 100 s, and processes that respond in > 1000 s. We suggest that the fast response corresponds to the current following the load at nearly constant membrane water content. The 100 s response time corresponds to the adjustment of membrane water content by diffusion. The long time response of 10^3–10^4 s corresponds to water absorption or desorption from the membrane and mechanical relaxation processes of the membrane.

The polarization curves in Fig. 3A represent steady state operation; the discontinuity in the polarization curve is unusual, and has not been previously observed. Because water is a product of the fuel cell reaction, it is necessary to wait after a step change in the load resistance for the water content in the membrane to equilibrate with the production and removal of water. As shown in Figs. 3B and C it can take a very long time for this steady state to be established.

We stress the importance of distinguishing steady states during testing of PEM fuel cells. The dynamics of transitions between steady states shown in Fig. 3 show that it took 10^3–10^4 s for a new steady state to be established after changing the external load resistance. Obtaining a steady state polarization curve requires hours to equilibrate at each load resistance. The polarization curves in Fig. 3A took more than 24 h to obtain. "Instantaneous" polarization curves may be obtained by sweeping the external load quickly, such that the differential water balance (difference in water produced by reaction and the water removed by convective flow) is negligible in comparison to the water inventory in the fuel cell. Polarization curves obtained in 1–2 min correspond to constant membrane water content; these are "instantaneous" polarization curves, not steady state polarization curves.

The transitions between steady states were repeated more than ten times over a period of four weeks and were highly reproducible. We were also able to reproduce the hysteresis with two different MEAs. The transitions between the low water content and high water content steady states were examined in more detail. The relative humidity in the cathode and anode effluents was monitored simultaneously with the current after changing the external load resistance. As seen in Figs. 3B and C the relative humidity at both the anode and cathode changed concurrently with the fuel cell current. When the current increased in response to decreasing the load resistance, the relative humidity at the cathode increased at the same time; the increase in relative humidity at the anode lagged the increase in the current by ~ 100 s. The time lag between the change in anode humidity and change in current was repeated when the current jumped after 1500 s. (The relative humidities shown in Fig. 3 are the values measured at the sensors; these values have not been corrected for the temperature difference between the fuel cell and the sensor, the effluent flow rates, and the water partitioning between the anode and cathode. The important feature of these data is the temporal correlation between relative humidity and fuel cell current.)

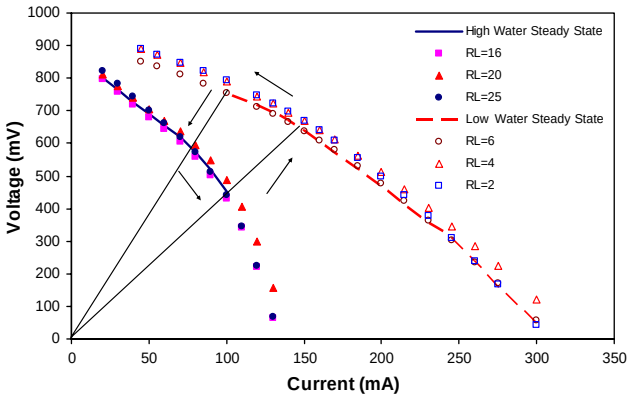

Fig. 4. Steady state and "Instantaneous" polarization curves of the autohumidification STR PEM fuel cell at 80 °C. The dashed line is the *steady state* polarization curve starting from equilibration with a low load resistance (2 Ω). After equilibration the load resistance is swept from 0 to 20 Ω at 1 Ω/4 h to obtain the polarization curve. The solid line is the *steady state* polarization curve starting from equilibration at a high load resistance (20 Ω). The data points correspond to "instantaneous" polarization curves, where the MEA water content is constant. The fuel cell was equilibrated for 4 h with load resistance specified and then the "instantaneous" polarization curve was obtained by sweeping the load resistance from 0 to 20 Ω at 0.2 Ω/s.

The relative humidity measurements also tracked the cell current when the load resistance was switched from a low load to a high load. The change in anode relative humidity was coincident with the decrease in current, while the relative humidity at the cathode lagged the decrease in current.

The existence of multiple ignited states with the PEM fuel cell was surprising. To understand how this phenomenon was affected by temperature, steady state polarization data were obtained at fuel cell temperatures of 50, 65, 80 and 95 °C. The procedure was time consuming: the load resistance was changed stepwise by $\sim 1\,\Omega$ every 4 h and steady state current and voltage were recorded. "Instantaneous" polarization curves were also recorded at constant water content before each step change in the load resistance. The "instantaneous" polarization curves were recorded by sweeping the load resistance from 0.2 to 20 Ω over a period of < 100 s.

Two stable "ignited" steady states were only observed at 80 and 95 °C; at 65 and 50 °C only a single ignited steady state was observed in our studies. Hysteresis loops were observed at 80 and 95 °C. Fig. 4 shows the steady state polarization curves at 80 °C; also plotted are data for a number of the "instantaneous" polarization curves obtained at "constant water content". The "instantaneous" data are nearly coincident with either the low water content or high water content branches of the steady state polarization curves, and show a smooth extension of the two branches beyond the region where they are long-term stable. If the load resistance is maintained in the extension region, the fuel cell current and voltage will eventually transition to the steady state values.

The data indicate that, at steady state, the MEA exists in distinct states of hydration, and the membrane steady state water content does not change smoothly with load resistance.

5. Long-term fuel cell performance

The first MEA we employed in the STR PEM fuel cell lasted ∼2000 h; the fuel cell failed when the membrane ripped during operation. After two design changes to the flow channels we replaced the MEA and the fuel cell was operated in the autohumidification mode continuously for a period of ∼ 12, 000 h with the same MEA (this was the third MEA). With the third MEA we observed changes in the fuel cell performance characteristics over the course of 18 months of operation. During the first 2500 h the fuel cell operated consistently and reproducibly. Both the "instantaneous'' and the steady state current/voltage responses were reproducible to within 2–3%. The performance was also similar to that observed with the first MEA, with current/voltage responses being reproducible between the two MEAs to within 15%. After approximately 3000 h of continuous operation the fuel cell began to exhibit various and sundry complexities. Under fixed operating parameters the fuel cell displayed oscillatory and/or chaotic changes in current and voltage. The fuel cell current for the same flow rates, temperature, and external load resistance declined by a factor of 10 between 5000 and 10,000 h of operation. Because we were not anticipating all this unusual behavior we did not record a complete systematic history of these changes. However, we report a number of specific results that illustrate the complex dynamics of PEM fuel cell operation.

After ∼3000 h of operation some of the "instantaneous'' polarization data showed anomalous points that did not coincide with data previously obtained. To identify what might have changed, "stationary'' state (fixed control parameters) data were recorded, where the feed flow rates and composition, the fuel cell temperature and the external load resistance were fixed and the current, voltage and relative humidity of the effluents were recorded over 24 h. Fig. 5 shows a set of stationary states currents recorded at 80 °C with flow rates of 10 mL/min H_2 at the anode and 10 mL/min O_2 at the cathode and the external load resistance set as indicated. At the low load resistance the current is apparently chaotic, showing irregular jumps. As the load resistance was increased the apparent chaotic behavior was damped out and above 4.8 Ω the current was stable. The relative humidity is not shown; it also fluctuated irregularly, but correlated with the current. The relative humidity was always below 75%, ruling out the possibility of liquid water flooding the cathode (flooding of the cathode should decrease the current, which is opposite of what was observed).

To further rule out water flooding, the same experiment was carried out with humidified feed streams. The feed streams were passed through bubblers held at 22 °C. The relative humidity of the feed streams at the cell temperature

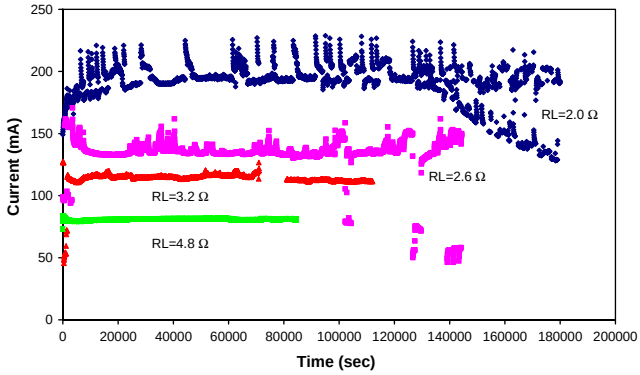

Fig. 5. Irregular performance of the STR PEM fuel cell under stationary conditions. The fuel cell was operated with dry feeds of 10 mL/min H_2 and 10 mL/min O_2 at 80 °C. The external load resistance was as set as shown. These data were collected after 3000 h of continuous fuel cell operation.

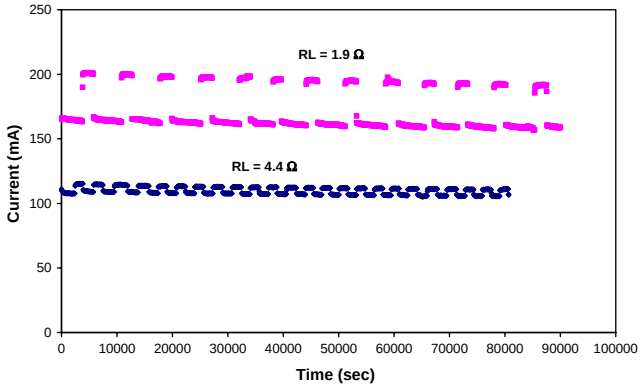

Fig. 6. Fuel cell performance of STR PEM fuel cell under stationary conditions with feed humidification. The fuel cell was operated with the feed streams of 10 mL/min H_2 and 10 mL/min O_2 humidified to 5%RH at 80 °C. The external load resistance was set as shown. These data were collected after the MEA had been in continuous use for 3000 h.

of 80 °C was ∼5%. Fig. 6 shows the stationary state performance of the STR PEM fuel cell with similar conditions shown in Fig. 5, but with the feed humidified to 5%. The chaotic fluctuations now became regular autonomous oscillations. The period of the oscillations was long, 6200 s when the load resistance was 1.9 Ω and 3300 s when the load resistance was 4.8 Ω. The magnitude of the oscillations scaled inversely with the load resistance, the largest oscillations being observed at the lowest load resistance.

The stationary state operation at 65 °C with the feed streams humidified is shown in Fig. 7. The feeds were still humidified at 22 °C, so the relative humidity of the inlet streams was ∼11% at the lower cell temperature. Regular oscillations were observed, but the oscillation period was longer at the lower temperature.

After the STR PEM fuel cell had been operated continuously for over 5000 h the fuel cell started displaying autonomous oscillations under virtually all conditions of

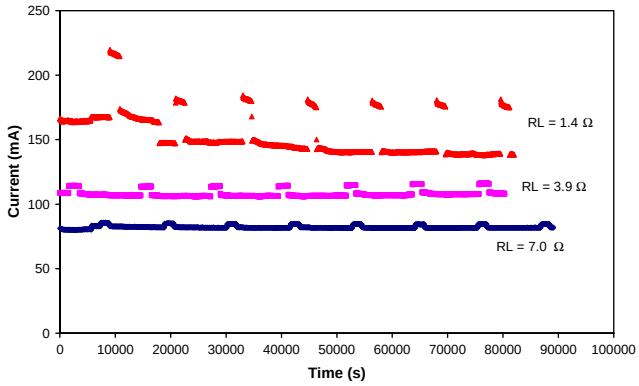

Fig. 7. Fuel cell performance of STR PEM fuel cell under stationary conditions with feed humidification. The fuel cell was operated with the feed streams of 10 mL/min H_2 and 10 mL/min O_2 humidified to 11%RH at 65 °C. The external load resistance was set as shown. These data were collected after the MEA had been in continuous use for 3000 h.

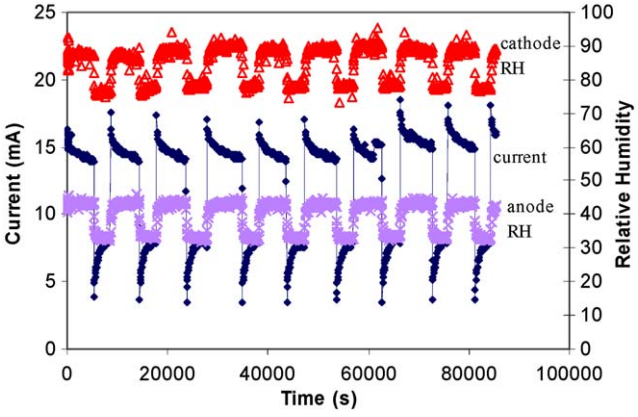

Fig. 8. Characteristic autonomous oscillations observed with the STR PEM fuel cell during 5000–12,000 h of operation. These are stationary states. The feeds were dry with flow rates 10 mL/min H_2, 10 mL/min O_2. The cell temperature is 80 °C, with a load resistance of 10 Ω.

temperature, feed flow rate, feed humidification and external load resistance. For temperatures between 50 and 100 °C with external load resistances varying from 0.2 to 20 Ω the system would settle into a state of autonomous oscillations after 24 h. Current, voltage and relative humidity of the anode and cathode effluents were monitored over a broad range of conditions, and autonomous oscillations persisted for 7000 h. (The STR PEM fuel cell operated continuously for 12,000 h.) During the time period between 5000 and 12,000 h of operation the oscillations had a very regular characteristic shape as shown in Fig. 8.

The current and voltage show regular relaxation oscillations, resembling the opening and closing of a capacitive switch. The oscillations abruptly rise then decay to a high current plateau; after a period of several thousand seconds the current or voltage precipitously drops, and then rises to approach a low current or voltage. The relative humidity of the anode and cathode effluents tracks the rise and fall of the

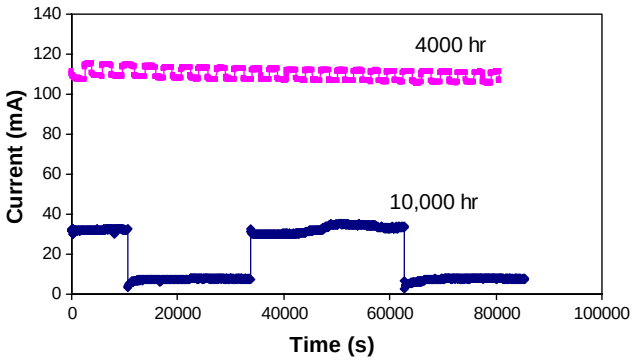

Fig. 9. A comparison of the oscillations in the STR PEM fuel cell at stationary state. Both runs were done at 80 °C with dry feeds of 10 mL/min H_2 at the anode, 10 mL/min O_2 at the cathode. The load resistance was 4.4 Ω for the 4000 h test and 4.1 Ω for the 10,000 h test.

current oscillations. The cathode effluent relative humidity rises coincident with the current increase. There is a time delay of ∼100 s from the current increase until the relative humidity at the anode starts rising.

During the extended fuel cell operation from 5000 to 12,000 h the performance of the fuel cell slowly changed. The periods of the autonomous oscillations lengthened and the current and voltage decreased at the same fixed control parameters (temperature, feed flow rates and load resistance). Over short periods of times of ∼100–200 h the fuel cell performance did not change appreciably, and we could treat it as quasi-stationary. Fig. 9 shows this quasi-stationary state operation of the fuel cell at 80 °C with a load resistance of 4 Ω after 4000 h of operation and again after 10,000 h of operation. Oscillations are evident in both cases. The amplitude of the current oscillations has increased over time from 6 to 22 mA. The period of the oscillations increased substantially from 3000 to 22,000 s, and the baseline for the current decreased from 110 to 10 mA. When this work was started we did not plan to study aging phenomena over an extended period of operation, so our data are not complete. The results suggest that the STR PEM fuel cell can be helpful and provide a simple and effective method to follow aging phenomena for MEAs.

6. Discussion

The STR PEM fuel cell was operated continuously for ∼12,000 h; temperature, flow rates, and external load resistance were all varied over that time period. Most of the time the fuel cell was operated in the autohumidification mode; the feed was humidified for a total of ∼300–400 h. The fuel cell performance evolved through three stages of operation.

1. For the first 2000 h of operation the fuel cell exhibited time invariant steady states. Steady state multiplicity was observed. The fuel cell current was extinguished when the initial water content of the membrane was below

$\sim$1.6 H_2O/SO_3. At higher initial water contents the fuel cell ignited and operated with autohumidification. Above 70 °C two stable "ignited'' states were observed.
2. During the extended time period 2500–3500 h the fuel cell began to display combinations of apparently chaotic and periodic variations of system variables for constant values of the input parameters.
3. After 5000 h the fuel cell displayed regular periodic variations of system variables with all combinations of input parameters. After making any change to the system parameters, the fuel cell system variables would approach steady autonomous oscillations within 24 h and the oscillations would persist indefinitely. The open circuit voltage declined slowly, but steadily, going from $\sim$0.92 V at 5000 h to $\sim$0.25 V at 10,000 h.

The operation of the STR PEM fuel cell revealed unusual dynamics.

1. Hysteresis between two stable ignited states, with the steady state selected depending on the initial conditions of the fuel cell.
2. Responses of the current, voltage and effluent relative humidity to changes in external load occurring on at least three different times scales from $\sim$1 to $\sim$10,000 s.
3. Autonomous oscillations with time constants $\sim 10^3$–10^4 s consisting of abrupt changes between almost stationary states.
4. Changes in the dynamic performance of the fuel cell with membrane ageing.

The extended range of operating parameters we studied here revealed complexities in the dynamical operation of a PEM fuel cell that have not been previously reported in the literature. We believe the complex phenomena we reported here result from a coupling of the mechanical, chemical and electrical properties of the PEM.

6.1. Steady state in PEM fuel cells

Fig. 3 reveals that it takes a long time to achieve steady state in PEM fuel cells. It can take thousands of seconds for the current and voltage to stabilize after a change in the external load resistance. One reason for these slow dynamics of PEM fuel cells is that the membrane acts as a reservoir for water. The water content of the membrane must equilibrate with the water production and water removal rates from the fuel cell. A lower estimate of the equilibration time is the water absorption time, τ_{ab}. This time is equal to the capacity of the membrane to absorb water divided by the water production rate.

$$\tau_{ab} = \frac{(\text{sulfonic acid density})(\text{change in " waters per } SO_3\text{"})}{\text{current d}/2} \approx \frac{5\Delta\lambda}{j}\, s. \quad (4)$$

The absorption capacity depends on both the equivalent weight of the polymer (number of acid residues per unit mass), the thickness of the membrane and the number of waters absorbed per acid residue, λ. For current densities $\sim 100\,mA/cm^2$ and a change in the hydration state of the sulfonic acids of 1 water molecule per SO_3, the lower limit on the characteristic time is 100 s in a Nafion®115 membrane (assuming all the water formed is absorbed into the membrane). We observed much longer response times, suggesting additional complexities associated with transport and equilibration of the membrane to water production.

Figs. 3A and 4 show two distinct "ignited'' steady states. There were also two distinct "instantaneous'' polarization curves. The water content of the fuel cell effluents along an "instantaneous'' polarization curve was approximately constant indicating the membrane existed in one of two states of hydration.

The steady state water balance shown in Fig. 1 only accounts for a single "ignited'' state, and is not adequate to represent the experimental data for temperatures above 70 °C where two "ignited'' states were observed for intermediate load resistances. We employed the steady state current, voltage and relative humidity measurements to formulate an experimentally determined water production and water removal balance, analogous to the curves shown in Fig. 1, for conditions where *three stable steady states* exist.

The construction of the water production curve at 95 °C is illustrated in Fig. 10A. The steady state currents at different load resistances are shown as horizontal lines. For load resistances of 1.0–5.6 Ω the stable steady state corresponded to the high membrane water content branch; these states are designated by the solid horizontal lines at the upper right side of Fig. 10A. At load resistances of 8.5–15 Ω only the low membrane water content branch was stable; these are designated by solid horizontal lines at the lower left of Fig. 10A. When the load resistance was between 6 and 8 Ω (6.8 and 7.5 Ω), both the high and low branch were observed, and the steady state selected depended on the direction of approach. This middle region corresponds to where the hysteresis loop was observed; dashed horizontal lines designate the currents corresponding to those steady states.

The membrane water activity corresponding to each of these steady states was estimated from the relative humidity of the effluent streams. If mass transport across the catalyst and gas diffusion layers is fast, then the water activity in the membrane will be in equilibrium with the water activity in the effluent streams. We estimated the water activity in the membrane to be equal to the water activity in the cathode effluent; this estimate is probably low, as there will be some mass transport resistance across between the membrane and the gas flow channels. The estimated water activity is shown with a cross on the horizontal lines. These crosses represent the experimentally determined steady state currents as a function of membrane water activity.

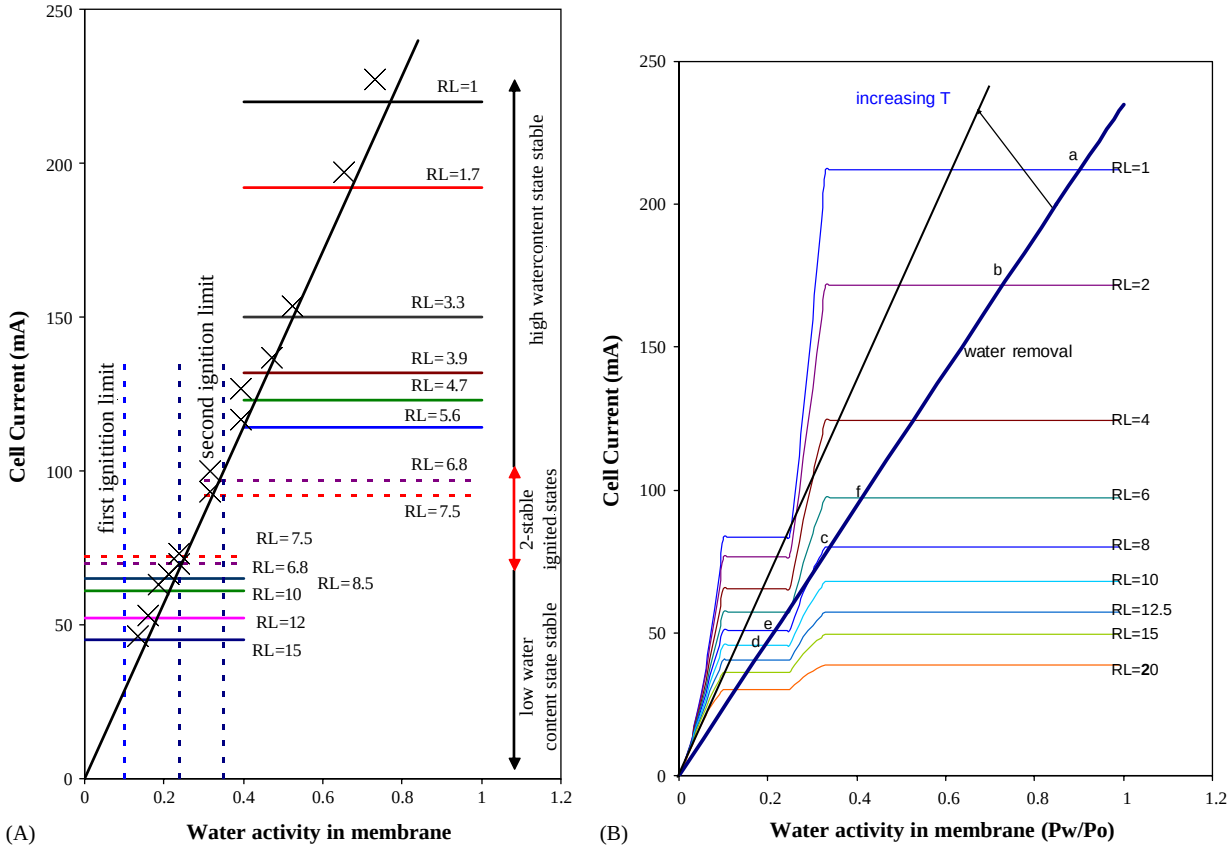

Fig. 10. (A) Construction of the approximate water generation curves for the autohumidification PEM fuel cell. The horizontal lines represent the experimentally observed steady state currents. First and second ignition ranges were set by limits on the membrane water activity for the low and high water content steady states. The X's represent estimated water activities based on the relative humidity of the cathode effluent. (B) Approximate water production and water removal for an autohumidification PEM fuel cell at 95 °C. The water generation curves were based on Eq. (1), with an effective voltage, $V' = 0.87$ and the membrane resistivity given by Eq. (5). Points labeled a–f, referred to in the text, represent a path around the hysteresis loop shown in Fig. 3A.

Two ignitions were observed. The first ignition separates the extinguished operation from "low water content" operation. The second ignition is the transition between the low membrane water content state and the high membrane water content state. The membrane water activity for the first ignition must be greater than zero and less than the membrane water activity of the low water content ignited state. The membrane water activity for the first ignition point was estimated to be < 0.10 from the relative humidity of the cathode effluent with a load resistance of 25 Ω. From direct measurements of fuel cell ignition at 50 °C the water activity for autohumidification ignition was ~0.06 (Moxley et al., 2003).

The second ignition is bounded by the membrane water activities of the "low" and of the "high" water content states. The lower limit is estimated from the cathode effluent relative humidity at the lowest resistance tested where the low water content branch is marginally stable ($R_L = 8.5\,\Omega$; $a_w \sim 0.25$). The upper limit is estimated by the anode effluent relative humidity at the highest resistance tested where the high water content branch is marginally stable ($R_L = 5.6\,\Omega$; $a_w \sim 0.33$).

The water production curves for a fixed load resistance, R_L, must start from near zero current for a dry membrane ($i \sim 0$; $a_w = 0$) and rise quickly to the current for the "low" water content branch at the first ignition point. We chose a functional form that fit the resistivity of Nafion as a function of relative humidity ($i \sim \exp(a_w^n)$; $0 < a_w < 0.10$). Because the polarization curve is nearly independent of the effluent relative humidity between the first and second ignition, the membrane resistance must remain nearly constant between the first and second ignition points ($i =$ constant; $0.10 < a_w < 0.25$). At the second ignition point, the water production curve must increase rapidly to the current for the high water content branch. We chose to represent this rapid increase over the range of the second ignition point as an exponential ($i \sim \exp((a_w - 0.15)^n)$; $0.25 < a_w < 0.33$). After the second ignition the "instantaneous" polarization curve is again nearly independent of the effluent relative humidity, so the membrane resistance must remain nearly constant for membrane water activities greater than the second ignition point ($i =$ constant; $0.33 < a_w$). The membrane resistivity as a function of membrane water activity that fits the experi-

mental data is finally approximated by Eq. (5).

$$\rho(\Omega\text{-cm}) = \begin{cases} 10^7 \exp(-14 a_w^{0.2}), & a_w < 0.1, \\ 1450, & 0.1 < a_w < 0.25, \\ 10^7 \exp(-14(a_w - 0.15)^{0.2}), & 0.25 < a_w < 0.33, \\ 48, & 0.33 < a_w. \end{cases} \quad (5)$$

The water removal line is approximately a straight line that starts at the origin and intersects the water production curves at the steady state currents. The water removal line is sketched in Fig. 10A; we have shown it passing slightly to the right of the plotted steady state points to reflect that the water activity of the cathode effluent is an underestimate of the membrane water activity.

We constructed the water production curves shown in Fig. 10B based on the right-hand side of Eq. (1) using an effective voltage of 0.87 V and employing Eq. (5) for the membrane resistance.

Fig. 10B can rationalize the hysteresis loops presented in Fig. 3. Consider a fuel cell operating at steady state with a load resistance of 1 Ω; the fuel cell will be in the high water content steady state with a cell current of 220 mA (point a). Increasing the load resistance to 2 Ω will result in a decrease in the cell current to 175 mA, but the cell continues to operate in the high water content state (point b). As the load resistance is increased to 8 Ω the current will decrease smoothly to 80 mA (point c). When the load resistance is increased to 10 Ω the high water content state no longer exists. After increasing the resistance to 10 Ω the current will temporarily decrease to 68 mA (the current that would correspond to "constant water content"). This current corresponds to extending the high current branch of the $R_L = 10\,\Omega$ line into the region where it is no longer at steady state. Eventually, the water level in the membrane decreases and the current will drop to 52 mA where it will be in steady state at the low water content steady state (point d). Increasing the load resistance further will cause the current to drop smoothly, but always in the low water content state. If the load resistance is decreased from 10 to 8 Ω the cell current will increase from 52 to 60 mA (point e). The fuel cell will continue to operate on the low water content branch until the resistance is reduced to 6 Ω. When the resistance is decreased to 6 Ω the low water content state no longer exists; the current will temporarily increase to 75 mA (the current that would correspond to "constant water content") and eventually it will jump to 100 mA to its new stable steady state (point f). The data shown in Figs. 3B and C correspond to the dynamics of these jumps.

The membrane resistance as a function of water activity given by Eq. (5) suggests that the steady state water content in the membrane changes abruptly with water activity. The five steady states (three stable) and hysteresis loop were only observed at 80 and 95 °C, but not at lower temperatures. Fig. 11 shows the MEA resistance (determined from the minimum slope of the "constant water content" polarization curve) as a function of cell temperature for both the low water content state and the high water content state. The MEA resistances for the two branches diverge above 65 °C.

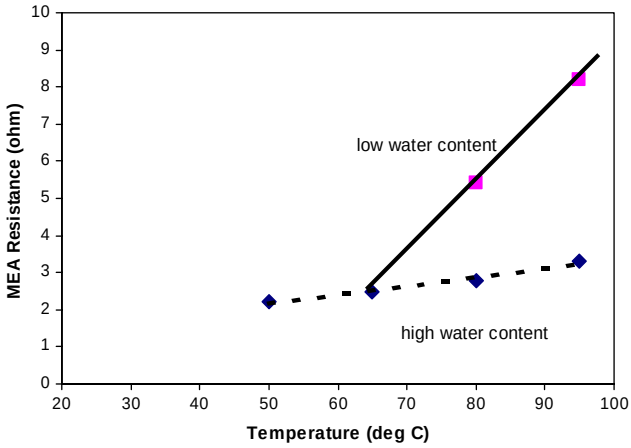

Fig. 11. Effective MEA resistance for the low and high water content steady states in the STR PEM fuel cell. At $T < 65$ °C only a single ignited steady state was observed. The MEA resistance was determined from the minimum slope of the polarization curve in the ohmic region.

6.2. Mechanical properties of membranes and fuel cell operation

Why should the five steady states appear above a "minimum temperature", and why does the membrane resistance change abruptly with water activity? We advance the conjecture that the three stable steady states and the stepwise decrease in the membrane resistance result from a coupling of mechanical and chemical effects. The polymer membrane in the MEA is pressed between the graphite plates (with the gas flow channels) and the porous carbon electrodes, spatially confining the membrane. As the membrane takes up water, the proton conductivity increases, but the membrane must also swell. However, being spatially confined, the membrane is not free to swell; it must do work to push the electrodes apart, or to swell *into* the porous electrode. Water uptake is hindered by these spatial constraints, just like the absorption of water by a sponge is restricted when the sponge is confined between two plates. The energy required for swelling (or shrinking) of the membrane depends on the *material properties* of the membrane. Increasing temperature and increasing water content both reduce the elastic modulus of the Nafion membrane. Additionally, the glass transition temperature of Nafion decreases with water content, which dramatically alters the elastic modulus. Above a critical temperature and membrane water content, the swelling pressure of the membrane is reduced to the point where it is not sufficient to push the electrodes apart and absorb more water.

The effect of the spatially confined MEA on the water uptake is to "pin" the membrane water content at fixed values until the membrane swelling pressure becomes sufficient to

overcome the applied force of the electrodes. By pinning the water content, the proton conductivity is also effectively pinned. This results in the membrane resistance as represented by Eq. (5).

Proton conductivity in Nafion as a function of applied pressure has been studied, but these studies have been at constant water content, where the water was confined to the membrane and could not be desorbed (Bendler et al., 2002, 2003; Serpico et al., 2002). In the fuel cell the membrane is constrained but is in contact with the vapor phase. Water will move between the membrane and the gas phase until chemical equilibrium is achieved. The water content in the fuel cell membrane is determined by the vapor phase water activity. Applying pressure to the membrane by clamping it in the fuel cell will squeeze water from the membrane. A membrane clamped between electrodes will have a lower water content and lower proton conductivity than a membrane which is free to swell.

The pressure loading of PEM electrodes may play a critical role in the performance of PEM fuel cells, and this subject will be vital to proper design and control of PEM fuel cell stacks where both temperature and water activity dynamically vary. Reports exist of considerable variability of the performance of individual cells in PEM stacks (Lee et al., 2002; Dante et al., 2003; Van Nguyen and Knobbe, 2003). A contributing factor to this variability could be the clamping pressure on the MEA in each cell, which would limit the water uptake and create variable steady state membrane resistances.

We tested the possibility of altering the membrane water content with pressure by altering the sealing pressure on the MEA in the fuel cell. The STR PEM fuel cell was operated at 80 °C, with dry feeds of 10 mL/min H_2 and 10 mL/min O_2. The sealing pressure on the cell was set by finger tightening the bolts, and then stepwise tightening of the bolts and measuring the degrees turning the bolts (we used 8/32 bolts so 360° corresponds to 1/32 of an inch compression, 0.8 mm). After each successive tightening of the bolts the fuel cell was allowed to stabilize for 3–4 h with an external load resistance of 2 Ω, and then a polarization curve was obtained. The MEA resistance was estimated as the minimum slope of the "instantaneous" polarization curve. In Fig. 12B we plot the MEA resistance as a function of the sealing on the MEA. (Because there are multiple layers of materials in the electrode and a sealing gasket, it is not possible with this simple experiment to determine the actual pressure applied to the membrane.) The initial decrease in the MEA resistance results from improving the membrane–electrode contact reducing the interfacial resistance. The MEA resistance goes through a minimum and then increases as the bolts are tightened further. Lee et al. (1999b) obtained similar results showing a greater voltage decrease with current as the compression on the fuel cell was increased (Lee et al., 1999a). We attribute the eventual increase in MEA resistance with increased compression to water being squeezed out of the membrane.

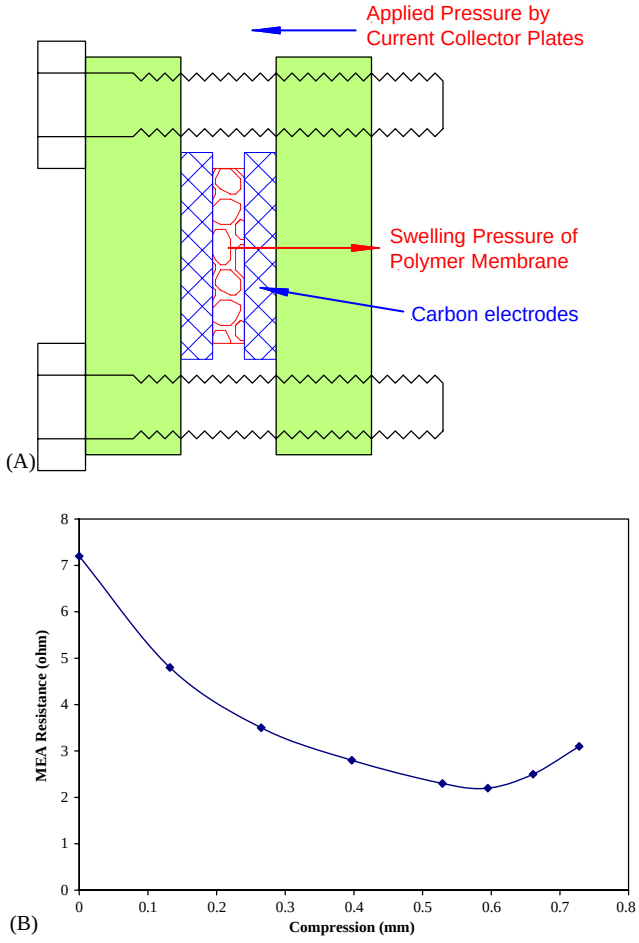

Fig. 12. (A) Schematic of the sealing of the MEA in the STR PEM fuel cell. (B) Effective MEA resistance as a function of sealing pressure on the MEA. The bolts on the plates sealing the MEA were tightened to figure tight, and then the compressed further. The MEA resistance was determined from the minimum slope of the polarization curve in the ohmic region.

6.3. Oscillations and chaos

When irregular, apparently chaotic dynamics of the fuel cell current were first observed, it was thought that condensation and evaporation of liquid water may be responsible. At low temperatures (below 50 °C) and low load resistance we saw that the fuel cell current dropped precipitously after a couple of hours of operation. However, under those conditions the relative humidity sensor in the cathode effluent was pegged at 100% and liquid water dripped from the cathode effluent. When the high temperature oscillations reported here were observed, the relative humidity sensors were recording values ∼40% RH, and there was no evidence of liquid water. When the oscillations became regular, they appeared to jump between conditions previously identified as stable steady states.

The apparently chaotic current variations and the autonomous oscillations were not observed during the first

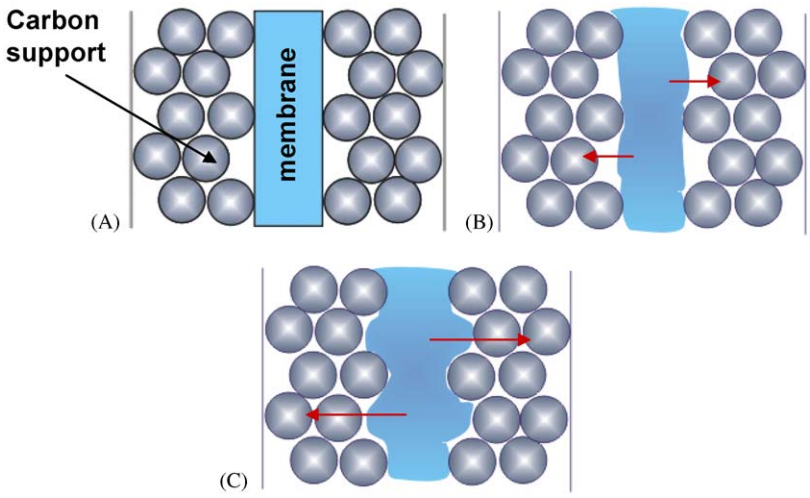

Fig. 13. Membrane swelling and the interfacial contact of the electrode and membrane. (A) The membrane initially contacts the top layer of carbon particles. (B) As the membrane takes up water it swells and pushes into the gaps of the catalyst particles, (C) eventually touching the second layer of catalyst particles.

3000 h of operation of the STR PEM fuel cell; we attribute the change is dynamic behavior to long-term physical changes of the MEA that occur gradually over time. The mechanical properties of the membrane slowly degrade from a combination of mechanical stressing and oxidative degradation reactions at the cathode. The evolution of the stable steady states into oscillations suggests that the membrane may become more elastic during the aging process.

The current oscillations exhibit abrupt transitions. A close look at Fig. 8 shows that the current oscillations have the dynamic characteristics of a capacitive switch with overshoot of the high state and undershoot of the low state. The relative humidity of the effluent streams also changes abruptly in phase with the current oscillations.

Why are the transitions between states so abrupt? We suspect that membrane swelling and relaxation processes create an interfacial contact switch between the membrane and the electrode. We propose a very simple model for this process. The electrode is composed of micron sized carbon particles, on which Pt nanoparticles are supported. The particles are fused together with binder material and coated onto a woven cloth. The membrane has a smooth surface and contacts the outermost layer of catalyst particles, as suggested in Fig. 13(A). As the membrane absorbs water it swells, extruding in the gap between the carbon particles. After it swells sufficiently, it contacts the second layer of catalyst particles, as suggested in Fig. 13(C). When contact is made with the second layer of catalyst particles, the interfacial resistance drops by almost a factor of two and the current jumps up. The capacitive double layer of protons that builds up on the catalyst particles is discharged when contact is made, which may explain the spike and decay of the current seen in Fig. 8. The swollen membrane is stressed; the corrugation of the membrane surface is a high energy state. Stress relaxation of the polymer causes the extruded dimples touching the second layer of catalyst to slowly relax and stretch out in the plane of the membrane. When it breaks contact with the second layer of catalyst particle, the current drops and the water content in the membrane starts to decrease. Some of the protons are drawn off to replenish the double layer, conceivably causing the current undershot.

Large jumps in the fuel cell current, similar to the "chaotic" behavior reported here have been reported by Lee et al. (1999b) and Atkins et al. (2004). Both sets of investigators observed large current or voltage fluctuations in an integral PEM fuel cell with serpentine flow channels when the cathode feed was dry and the anode feed was humidified to $< 70\%$ RH. As they increased the anode humidification the fluctuations died out. We suggest that this type of fuel cell behavior at reduced water activity is the result of membrane swelling and changes in interfacial contact. The integral PEM fuel cells show more complex behavior because of additional complications of spatial variations along the flow channels.

While the physics behind the oscillations are not well understood, we speculate that the phenomena arise from the coupling of the mechanical properties of the polymer with its chemical and electrical properties. The mechanical properties of ionomers, such as Nafion, are functions of the temperature and the membrane water content. One possible explanation for the oscillations is that the changes in membrane water content cause the glass transition temperature of the membrane to oscillate around the fuel cell temperature. As water is formed the membrane swells and extrudes into the pores of the catalyst layer. As the membrane water content increases the elastic modulus will decrease and the polymer

will relax to reduce the strain from the extrusions into the catalyst pores. With the elastic modulus reduced the clamping pressure on the MEA will compress the polymer membrane, squeezing water out of the membrane. Eventually the membrane loses enough water and the modulus increases so the process repeats with the polymer again extruding into the gap between particles. We have no direct evidence for the proposed mechanism. But the characteristic stress relaxation time of Nafion at room temperature and ambient relative humidity was measured to be ∼3000 s, which correlates well with the period of the current oscillations (Satterfield, 2003).

6.4. Membrane aging

Our data show that the pathology of the PEM fuel cell dynamics gradually changes with time on-stream. Unfortunately, the existing experimental apparatus does not permit direct observations of the mechanical, chemical and electrical properties of the membrane and the membrane–electrode interface over the time periods of operation. Both the membrane's mechanical properties and the membrane–electrode interface are expected to experience the effects of aging. The onset of oscillations with time and the range of temperature and water content over which the oscillations occur suggest that the membrane possibly becomes "softer'' due to aging (i.e., the membrane behaves as if it were more elastic due to aging).

Both the cell voltage and cell current for the same load resistance decreased with time after 5000 h of operation. The open circuit voltage also decreased substantially, from 0.91 to 0.25 V, between 5000 and 10,000 h of operation. During the extended operation we also observed that we no longer had closure on the mass balances. There was substantially more water in the effluents from the anode and cathode than corresponded to the fuel cell current. For example, the data in Fig. 8 indicate that the water removed in the anode and cathode effluents was nearly four times the water formed by the fuel cell current. This suggests that aging leads to increased membrane permeability allowing greater cross-over of the reactants (molecular hydrogen and oxygen pass through the membrane where they react on the Pt catalyst almost instantaneously to form additional water). The increased membrane permeability can account for both the decreased open circuit voltage and the loss of mass balance.

We observed with one of our STR PEM fuel cell tests that the fuel cell failed after ∼2000 h of operation. The failure mode was a tear along one of the edges of the graphite flow channel plate where the stress to the MEA was greatest. With the continual stressing due to swelling, the membrane will fatigue. The points of greatest fatigue will be at the points where the MEA is fixed. Stressing may create microscopic stress fractures where the permeability of the reactant across the membrane may be much greater.

7. Implications for PEM fuel cells

The PEM fuel cell operating conditions reported here are unusual; almost all our results are at low relative humidity in the cell, most of them to relative humidity of $< 40\%$. We are not advocating operating a commercial PEM fuel cell in the mode or configuration we employed in our experiments. However, it is essential to know how a PEM fuel cell operates in all conditions to understand how to effectively control it under extremes of operation. *Operation of a PEM fuel cell under low humidification conditions accentuated the effects of membrane swelling and highlighted the impact of membrane mechanical properties*. Researchers at GM have recently been suggesting the desirability to operate PEM fuel cells with under-humidified feed streams (Mathias et al., 2004). The results reported here suggest there are many complexities with such operation, beyond the reduced proton conductivity.

The water content in the membrane depends on the water activity, but also on the applied mechanical pressure. In building fuel cell stacks it is essential to control both the pressure applied to the MEA and the humidification of the reactants feeds. In a large fuel cell with serpentine flow channels the variation of water activity along the length of the flow channel may result in differential mechanical stresses and highly non-uniform proton conductivity. *Cell-to-cell variability* in a stack may result from poorly controlled clamping of the bipolar plates. It is important not to over-tighten the clamping of the MEA assembly in PEM fuel cells since it can limit the membrane water uptake.

The importance of the membrane–electrode interface is well appreciated by fuel cell researchers. The results presented here indicate that the membrane–electrode interface evolves dynamically with membrane water content, temperature and time. There are multiple characteristic time scales associated with PEM fuel cells. The "constant membrane water content'' time scale is equal to 1 s. However, we have demonstrated here that there are two much longer time scales associated with PEM fuel cell response. It takes ∼100 s for the membrane water content to equilibrate with water production. This is an essential time constant for startup of a PEM fuel cell system and for large changes in load (such as going from idling to high speed driving). Mechanical property changes of the PEM resulting from changes in water content may require $\sim 10^4$ s to equilibrate. Such changes could be very disruptive to PEM fuel cell applications—it is critical to isolate the conditions for this phenomenon and avoid that region of operation. The membrane swelling due to water absorption should also alert us to the need for controlled pretreatment of PEM fuel cells. MEAs are generally made by hot pressing the membrane and electrode to get good adhesion (Raistrick, 1989; Uchida et al., 1996; Antolini et al., 1999). Contraction of the membrane with temperature after the hot pressing, and subsequent swelling of the membrane with water may significantly alter the interfacial contact and interfacial resistance. The dynamics of these pro-

cesses must be controlled; it would not be tolerable to have sudden changes in the power output from a PEM fuel cell due to changes in interfacial resistance.

We have been unable to find any reports in the literature of multiple steady states and autonomous oscillations in PEM fuel cell operation except in the presence of impurities in the feed (Zhang and Datta, 2002). This might lead to dismissal of the results presented here as being associated with esoteric phenomena only observed under highly unusual circumstances. We have received private communications from several companies involved with fuel cell development (Ballard, W.L. Gore), that report anomalous operation of PEM fuel cells with under-humidified feeds (U. Beuscher, pers. comm.; J. Kenna, Ballard Corp. pers. comm.). Lee et al. (1999b) have published results for under-humidified feeds that show "chaotic-type'' performance that is may also be rationalized along the lines we presented. Atkins et al. (2004) also found large current fluctuations in a PEM fuel cell operating with under-humidifed feeds (Atkins et al., 2004). We believe that the results from Lee et al. (1999b) and Atkins et al. (2004) are both manifestations of the same phenomena reported in this paper. We also suggest that the phenomena report here have been observed frequently, but were dismissed because they were not understood. Because most investigators employ a fuel cell test station with serpentine flow channels, the combination of spatial and temporal variations give complex fuel cell responses that are nearly impossible to deconvolve in detail. The simplified one-dimensional system we employed provides clear data that can be understood without the additional complexity of spatio-temporal variations. It is critical to understand the conditions where complexities such as "ignition points'' and oscillations occur, to design the control systems keeping operation away from those parameter regimes.

8. Conclusions

The dynamic response of a one-dimensional PEM fuel cell to changes in load exhibited steady state multiplicity, resulting from positive feedback between proton conduction in the membrane and water production from the fuel cell reaction. At temperatures above 70 °C two stable "ignited'' steady states were identified, with hysteresis between them. The two ignited states resulted from jumps in the membrane resistance with water activity, which we suggest is due to physical constraints of membrane swelling with water absorption. The sealing pressure of the electrodes to the membrane must be overcome by the membrane swelling pressure. If the clamping pressure of the fuel cell is too great, water will be excluded from the membrane, resulting in an increased membrane–electrode-assembly resistance.

The mechanical properties of the membrane gradually change over long-term operation, and stress relaxation of the swollen membrane may eventually lead to autonomous oscillations of the fuel cell current. These oscillations have a long period of ∼10,000 s and are dependent on temperature, water content and load resistance.

After 5000 h of continuous operation the open circuit voltage of the fuel cell began to decrease, and there was evidence of increased crossover of the reactants through the membrane.

These results strongly suggest the critical importance of the mechanical properties of the membrane for both the dynamic and steady state performance of a PEM fuel cell.

Notation

a_w	activity of water in the polymer membrane
D	gas phase diffusivity in gas flow channels $\sim 0.1\,\mathrm{cm}_2/\mathrm{s}$
$\mathscr{F}$	Faraday's constant, 96,468 coulombs/mol
F_A	molar flow rate at the anode, mol/s
F_C	molar flow rate at the cathode, mol/s
i_{H^+}	fuel cell current, amp
j	current density in polymer electrolyte, amp/cm^2
P_w^A	partial pressure of water at the anode, bar
P_w^C	partial pressure of water at the cathode, bar
P_{Total}	total gas pressure in the fuel cell, bar
P^0	vapor pressure of water at the fuel cell temperature, bar
Q	volumetric flow rate, cm^3/s
Q_A	volumetric flow rate at anode, cm^3/s
Q_C	volumetric flow rate at cathode, cm^3/s
R	gas constant, 82.06 cm^3-bar/mol-°K
RH	relative humidity, $P_w/P^0 \times 100$
R_m	membrane resistance, Ω
R_L	load resistance, Ω
T	fuel cell temperature
V	volume of gas flow channels, cm^3
V'	effective fuel cell voltage in ohmic polarization region, V
x_w^A	mole fraction of water in anode effluent
x_w^C	mole fraction of water in cathode effluent

Greek letters

λ	number of water molecules per sulfonic acid residue in the polymer electrolyte
ξ	fraction of water formed in the fuel cell exiting in the anode effluent

Acknowledgements

We thank the National Science Foundation (NSF grant CTS-0354279) and the Air Force Office of Scientific Research (Dynamics and Control Grant F49620-03-1-0097) for support of this work.

References

Antolini, E., Giorgi, L., et al., 1999. Influence of Nafion loading in the catalyst layer of gas-diffusion electrodes for PEFC. Journal of Power Sources 77 (2), 136–142.

Atkins, J.R., Savett, S.C., et al., 2004. Large-scale current fluctuations in PEM fuel cells operating with reduced feed stream humidification. Journal of Power Sources 128 (2), 201–207.

Bendler, J.T., Fontanella, J.J., et al., 2002. Anomalous defect diffusion near the glass transition. Chemical Physics 284 (1–2), 311–317.

Bendler, J.T., Fontanella, J.J., et al., 2003. Why conductivity decreases with pressure in ion-doped polymers. Fractals-Complex Geometry Patterns and Scaling in Nature and Society 11, 93–97.

Benziger, J.B., Chia, E., et al., 2004. A differential reactor polymer electrolyte membrane fuel cell. A.I.Ch.E. Journal 50 (8), 1889–1900.

Buchi, F.N., Srinivasan, S., 1997. Operating proton exchange membrane fuel cells without external humidification of the reactant gases—fundamental aspects. Journal of the Electrochemical Society 144 (8), 2767–2772.

Chia, E.-S.J., Benziger, J.B., et al., 2004. Water balance and multiplicity in a polymer electrolyte membrane fuel cell. A.I.Ch.E. Journal 50 (9), 2320–2324.

Dante, R.C., Escamilla, J.L., et al., 2003. Fractional factorial design of experiments for PEM fuel cell performances improvement. International Journal of Hydrogen Energy 28 (3), 343–348.

EG&G Services, P., Inc., 2000. Fuel Cell Handbook. US Department of Energy, Morgantown, WV, p. 312.

van Heerden, C., 1953. Autothermic processes: properties and reactor design. Industrial and Engineering Chemistry 45 (6), 1242–1247.

Lee, W.-k., Ho, C.-H., et al., 1999a. The effects of compression and gas diffusion layers on the performance of a PEM fuel cell. Journal of Power Sources 84, 45–51.

Lee, W.K., Van Zee, J.W., et al., 1999b. Effect of humidity on PEM fuel cell performance part I—experiments. International Mechanical Engineering Congress & Exposition, Nashville TN.

Lee, H.I., Lee, C.H., et al., 2002. Development of 1 kW class polymer electrolyte membrane fuel cell power generation system. Journal of Power Sources 107 (1), 110–119.

Mathias, M., Gasteiger, H., et al., 2004. Can available membranes and catalysts meet automotive PEFC requirements? 228 ACS National Meeting, Philadelphia PA.

Moxley, J.F., Tulyani, S., et al., 2003. Steady-state multiplicity in polymer electrolyte membrane fuel cells. Chemical Engineering Science 58, 4705–4708.

Raistrick, I.D., 1989. Electrode Assembly for Use in a Solid Polymer Electrolyte Fuel Cell. US Department of Energy, US.

Satterfield, M.B., 2003. Transport Through the Membrane–Electrode Interface in Polymer Electrolyte Membrane Fuel Cells. Princeton University; Princeton NJ, p. 45.

Serpico, J.M., Ehrenberg, S.G., et al., 2002. Transport and structural studies of sulfonated styrene-ethylene copolymer membranes. Macromolecules 35 (15), 5916–5921.

Springer, T.E., Zawodzinski, T.A., et al., 1991. Polymer electrolyte fuel-cell model. Journal of the Electrochemical Society 138 (8), 2334–2342.

Srinivasan, S., Dave, B.B., et al., 1993. Overview of fuel cell technology. In: Blomen, L.J.M.J., Mugerwa, M.N. (Eds.), Fuel Cell Systems. Plenum Press, New York, pp. 37–72.

Uchida, M., Fukuoka, Y., et al., 1996. Effects of microstructure of carbon support in the catalyst layer on the performance of polymer-electrolyte fuel cells. Journal of the Electrochemical Society 143 (7), 2245–2252.

Uppal, A., Ray, W.H., et al., 1974. Dynamic behavior of continuous stirred tank reactors. Chemical Engineering Science 29 (4), 967–985.

Van Nguyen, T., Knobbe, M.W., 2003. A liquid water management strategy for PEM fuel cell stacks. Journal of Power Sources 114 (1), 70–79.

Yang, C., Benziger, J., et al., 2004. A comparison of physical properties and fuel cell performance of nafion and zirconium phosphate/nafion composite membranes. Journal of Membrane Science 237, 145–161.

Zhang, J.X., Datta, R., 2002. Sustained potential oscillations in proton exchange membrane fuel cells with PtRu as anode catalyst. Journal of the Electrochemical Society 149 (11), A1423–A1431.